Brain Dynamics Through the Lens of Statistical Mechanics by Unifying Structure and Function

Igor Fortel[1], Mitchell Butler[1], Laura E. Korthauer[2,4], Liang Zhan[3], Olusola Ajilore[1], Ira Driscoll[2], Anastasios Sidiropoulos[1], Yanfu Zhang[3], Lei Guo[3], Heng Huang[3], Dan Schonfeld[1], and Alex Leow[1(✉)]

[1] University of Illinois at Chicago, Chicago, IL, USA
aleow@psch.uic.edu
[2] University of Wisconsin-Milwaukee, Milwaukee, WI, USA
[3] University of Pittsburgh, Pittsburgh, PA, USA
[4] Alpert Medical School of Brown University, Providence, RI, USA

Abstract. This paper introduces a novel method that unifies structural connectivity and functional time series to form a signed coupling interaction network or "signed resting state structural connectome" (signed rs-SC) to describe neural excitation and inhibition. We employ an energy representation of neural activity based on the Ising model from statistical mechanics, hereby bypassing traditional BOLD correlations. The spin model is a function of a coupling interaction (traditionally positive or negative) and spin-states of paired brain regions. Observed functional time series represent brain states over time. A maximum pseudolikelihood with a constraint is used to estimate the coupling interaction. The constraint is introduced as a penalty function such that the learned interactions are scaled relative to structural connectivity; the sign of the interactions may infer inhibition or excitation over an underlying structure. We evaluate our method by comparing a group of otherwise healthy APOE-e4 carriers with a control group of non APOE-e4 subjects. Our results identify a global shift in the excitation-inhibition balance of the APOE e4 signed rs-SC compared to the control group, providing the first connectomics-based support for hyperexcitation related to APOE e4.

Keywords: Ising model · Maximum Likelihood · Brain dynamics · Functional connectivity · Structure connectome · MRI

1 Introduction

The relationship between structure and function is an open question that some researchers have investigated using the Ising model from statistical mechanics [7,11,16,17]. Communication between neurons involves the release of certain neurotransmitters that drive an excitatory or inhibitory response. At a macroscopic level, this can be interpreted as a pair of brain regions having an activating

D. Shen et al. (Eds.): MICCAI 2019, LNCS 11768, pp. 503–511, 2019.
https://doi.org/10.1007/978-3-030-32254-0_56

or inhibiting influence on each other. It is hypothesized that a core abnormality of early AD is "hyperexcitability" in neuronal circuits, supported by recent whole-cell recordings in animal AD models demonstrating that β-Amyloid (Aβ) induces synaptic hyperexcitation and perturbs the excitation-inhibition (E-I) balance in regions such as the entorhinal cortex and anterior cingulate via depressing inhibitory transmission [14,15]. Our main contribution is a novel approach to evaluate this hypothesis, by computationally infering the nature (excitatory vs inhibitory) of structural connectivity using statistical mechanics to yield a signed interaction network or "signed resting state structural connectome" (signed rs-SC).

2 Ising Model

A functional connectome can be represented mathematically as an undirected graph where vertices (V) correspond to regions of interest (ROIs), and edges (E) describe some measure of connectivity between pairs of vertices. In conventional descriptions of functional connectivity (FC), each edge $e_{i,j} \in E$ is associated with a weight, computed using a pairwise BOLD correlation. In this work we use the Ising model, a special case of a Markov random field model in which each ROI can exhibit two possible states $s = \pm 1$. Previous studies have shown this to accurately model neuronal activity under the assumption that connectivity between neurons can either be active (+1) or inactive (–1) [16,18].

First, we formulate the system energy as given by the Hamiltonian $H(\mathbf{s}) = -\sum_{i<j} J_{i,j} s_i s_j \quad \forall\, i, j \in \{1, 2, \ldots, N\}$ where the spin configuration $\mathbf{s}$ is defined as the column vector $\mathbf{s} = [s_1, s_2, .., s_N]^T$, N is the number of regions, s_i and s_j are the spin states of region i and region j, and $J_{i,j}$ represents a pairwise interaction between those regions. This formulation is under the assumption that there is no external influence (i.e resting-state). Unless otherwise stated, summations in this paper are for $i < j$ to avoid double counting and exclude self-connections. The probability of observing a specific configuration is given by the Boltzmann distribution: $Pr(\mathbf{s}) = \frac{1}{Z} exp\,(-\beta H(\mathbf{s}))$, where β is the inverse temperature and Z is the partition function defined as $\mathrm{Z} = \sum_{\mathrm{s}} exp(-\beta H(\mathbf{s}))$. Here, the summation is over all possible configurations of states. Ising model simulation is described in algorithm 1 to find an equilibrium time evolution of states for each ROI [4]. Ising model dynamics have been previously used in multiple studies to estimate functional connectivity [6,11,17].

Our method aims to solve the "inverse problem", using observed functional time series to infer coupling interactions. Similar to previous work, we use a gradient ascent scheme [17,18]. However, where previous methods estimated network structure properties, we embed the structure into the estimation. This is achieved by using a gradient ascent procedure on the log likelihood of the observed data [1]. The computation of Maximum Likelihood, in this case, requires calculations over all 2^N possible spin configurations [12]. For large sample size, the pseudolikelihood (PL) approximation converges to the maximum likelihood with lower computational cost [3]. Ezaki et al. demonstrated the viability of a pseudolikelihood-based model to estimate features on functional time series [6].

Algorithm 1. Ising Model Simulations

1: Define: J, the maximum number of simulations σ, and a range of β values
2: **procedure** MONTE CARLO SIMULATIONS FOR EACH TEMPERATURE
3: Initialize: random configuration of spin states
4: for each simulation: randomly fix an element from the configuration, and compute the Hamiltonian relative to that fixed element, denoted by $H(\boldsymbol{s_i})$
5: if $H(\boldsymbol{s_i}) \leq 0$ or $rand(0,1) \leq exp(\frac{H(\boldsymbol{s_i})}{\beta})$, flip the state. The command $rand(0,1)$ generates a random value between 0 and 1. Complete for all states in configuration
6: The final configuration is used as the input to for next simulation
7: Concatenate all simulations into an $N - by - \sigma$ matrix and compute correlation by multiplying this matrix by its transpose and dividing by σ
8: Do this for each temperature in the range

3 Constrained Pseudolikelihood Estimation

We begin with the observed functional time series, which are binarized to be ± 1. A threshold of 0 is used for each sample due to the data being preprocessed with global signal regression (GSR) [9], resulting in a zero-mean time series; we binarize around the mean to avoid a bias towards either state. The resulting binary sequences represent the observed spin configurations, which we define as a function of the time samples: $\boldsymbol{S}_{observed} = [\boldsymbol{s}(1), \boldsymbol{s}(2), \ldots, \boldsymbol{s}(t_{\max})]$. We estimate a parameter $\mathbf{J}$, a set containing all $J_{i,j}$, via the maximization of the pseudolikelihood function, defined as:

$$\max_{\boldsymbol{J}} \mathcal{L}(\boldsymbol{J}, \beta), \ \textit{where } \mathcal{L}(\boldsymbol{J}, \beta) = \prod_{t=1}^{t_{\max}} \prod_{i=1}^{N} Pr\left(s_i(t) | \boldsymbol{J}, \beta, \boldsymbol{s}_{-i}(t)\right) \tag{1}$$

Unlike traditional Maximum Likelihood, the probability is not over all spin states, but of observing one $s_i(t)$ with all the others $\mathbf{s}_{-i}(t)$ fixed. To ensure the magnitude of the coupling interactions are scaled relative to the structural connectome, our constraint is formulated as $|J_{i,j}| = \mu W_{i,j}$, where μ is the normalization constant and $W_{i,j}$ is the structural connectivity between ROI pairs. With appropriate scaling, we assume that $\mu = 1$. We therefore pose a penalty-based optimization approach to maximize the log-pseudolikelihood function as follows:

$$\ell(\boldsymbol{J}, \beta) = \frac{1}{t_{\max}} \ln \mathcal{L}(\boldsymbol{J}, \beta) - \frac{1}{2} \lambda \sum_{i<j} \left(J_{i,j} - \operatorname{sgn}\left(J_{i,j}\right) W_{i,j}\right)^2 \tag{2}$$

We first evaluate the pseudolikelikelihood component $\frac{1}{t_{\max}} \ln \mathcal{L}(\boldsymbol{J}, \beta)$, which expands to: $\frac{1}{t_{\max}} \sum_{t=1}^{t_{\max}} \sum_{i=1}^{N} \ln \left(\frac{\exp\left(\beta \sum_{k=1}^{N} J_{i,k} s_i(t) s_k(t)\right)}{\exp\left(\beta \sum_{k=1}^{N} J_{i,k} s_k(t)\right) + \exp\left(-\beta \sum_{k=1}^{N} J_{i,k} s_k(t)\right)} \right)$. The probability distribution here stems from the Boltzmann distribution under the pseudolikelihood conditions such that the numerator of the log is the energy of the system, while the denominator is the sum of all possible energies. Thus,

only two terms are present in the denominator; one is positive and one is negative as $s_i(t)$ can only be $+1$ or -1. We can now simplify the likelihood function further by letting $C_i(t) = \beta \sum_{k=1}^{N} J_{i,k} s_k(t)$, which results in a formulation as follows:

$$\ell(\boldsymbol{J}, \beta) = \frac{1}{t_{\max}} \sum_{t=1}^{t_{\max}} \sum_{i=1}^{N} C_i(t) s_i(t) - \ln\left(\exp\left(C_i(t)\right) + \exp\left(-C_i(t)\right)\right) \tag{3}$$

$$-\frac{1}{2}\lambda \sum_{i<j} \left(J_{i,j} - \operatorname{sgn}\left(J_{i,j}\right) W_{i,j}\right)^2$$

The gradient ascent procedure can be constructed with respect to $J_{i,j}$ by computing the partial derivative of the constructed log-pseudolikelihood.

$$\frac{\partial \ell}{\partial J_{i,j}} = \frac{1}{t_{\max}} \sum_{t=1}^{t_{\max}} \beta \left\{ s_i(t) s_j(t) - s_j(t) \tanh\left(C_i(t)\right) \right\} - \lambda \left(J_{i,j} - \operatorname{sgn}\left(J_{i,j}\right) W_{i,j}\right) \tag{4}$$

where the updating scheme follows: $J_{i,j}^{n+1} = J_{i,j}^{n} + \epsilon \left.\frac{\partial \ell}{\partial J_{i,j}}\right|_{n}$ Here, n is the iteration number and ϵ is the learning rate. The partial derivative of the penalty holds under the assumption that $J_{i,j} \neq 0$ as the *sgn* function is continuous and constant everywhere except 0. In practice however, if there exists a $J_{i,j} = 0$, then $sgn(0) = 0$ by convention. The penalty function ensures that the inferred pairwise interaction is scaled relative to the estimated structure of the brain. To account for the β temperature constant we employ an alternating optimization strategy whereby we first assume $\beta = 1$ and compute the first step of the gradient ascent. Using the resulting coupling interaction, we can then optimize β by simulating the Ising model to find the temperature that yields the highest correlated result with the observed functional connectome. Using this new temperature we take the next step along the gradient and continue alternating between optimizing β and $J_{i,j}$ until the algorithm converges. Through simulations, we find that the optimal β is in the neighborhood of 1 for all subjects.

4 Results and Validation

Structural and functional connectivity for 38 cognitively normal Apoe-e4 carriers aged 40–60 ($\mu = 50.8$) are compared with 38 age ($\mu = 50.9$) and sex-matched (16M/22F) non-carriers (control). Imaging included T1-weighted MRI, resting state fMRI and diffusion weighted MRI. Freesurfer cortical parcellation and subcortical segmentation was performed to derive 80 ROIs. The mean time-course was extracted from the pre-processed rs-fMRI data. Probabilistic tractography was used to create the structural connectome matrices, and normalized by the way-total of the corresponding seed ROIs. More detailed information on the imaging and processing steps can be found in Korthauer et al. [9].

We first optimize λ in our constraint by estimating the coupling interactions $J_{i,j}$ for each subject using our method for a range of λ values. The estimated $J_{i,j}$

for each λ is then used to generate a correlation function $f_c(\beta)$ by simulating the Ising Model and computing the Pearson correlation between observed and simulated functional connectomes $\forall\beta$. The function $f_1(\lambda)$ contains the $max(f_c)$ achieved. To evaluate the impact of λ on our constraint, a second function $f_2(\lambda)$ computes the Pearson correlation between $|J_{i,j}|$ and $W_{i,j}$ $\forall$ i, j.

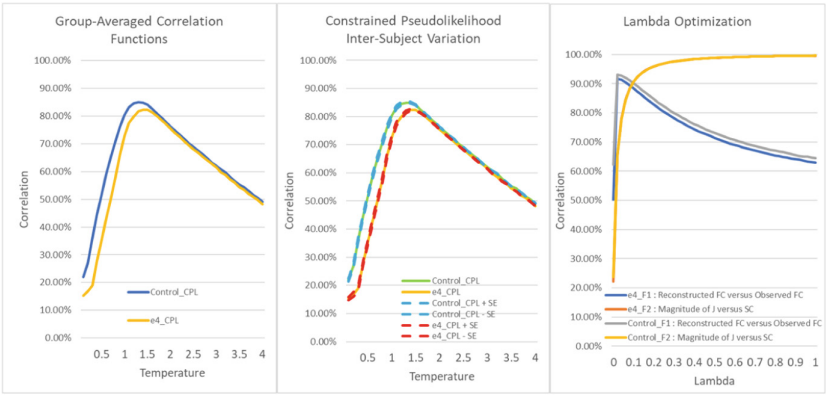

Fig. 1. Right: $f_1(\lambda)$ and $f_2(\lambda)$ curves are averaged over all 38 subjects in each group for $\lambda = (0, 0.05, ..., 1.00)$, where $\lambda = 0$ corresponds to the unconstrained case. Both groups are consistent, with optimal λ approximately 0.1. Left: f_c curve averaged over all 38 subjects in each group for $\beta = (0.05, 0.1, \ldots, 4.0)$ using 3 estimates for $J_{i,j}$, namely the constrained pseudolikelihood (CPL) with $\lambda = 0.1$, the unconstrained pseudolikelihood (PL), as well as simply using the structural connectome (SC) for $J_{i,j}$. Middle: f_c curve of the CPL case with standard error (SE) ribbon describing inter-subject variation

Group-averaged $f_1(\lambda)$ and $f_2(\lambda)$ are shown in Fig. 1. To determine an optimal λ, a min-max optimization is used: $D_r = arg\ \underset{\lambda}{min}(f_r(\lambda), r = (1, 2))\ and\ \lambda^* = arg\ \underset{D_r}{max}(\underset{\lambda}{min}(f_r(\lambda), r = (1, 2))$, corresponding to the intersection point between monotonically increasing and monotonically decreasing functions. We note that $f_1(\lambda)$ is not strictly monotonic due to the data point at $\lambda = 0$; however, the condition holds with that exception. We generate an f_c curve for each subject using 3 methods of determining the coupling interactions $J_{i.j}$: (1) our constrained pseudolikelihood estimation (CPL); (2) unconstrained pseudolikelihood estimation (PL); and (3) using the structural connectome as the coupling interaction (unsigned interactions). Shown in Fig. 1, f_c averaged over all subjects using the constrained model peaks at $\beta \approx 1$ and results in $r > 0.8$ at the maximum for both groups, while the other two are much lower. The improvement demonstrated by our method over the unconstrained estimate warrants further investigation into the effect coupling scale and time-series sample size may have on the result. For the control group, we show the similarity between group-averaged observed and simulated functional connectomes, and the coupling interaction and structural connectomes in Fig. 2, with correlation $r > 0.9$ for both comparisons.

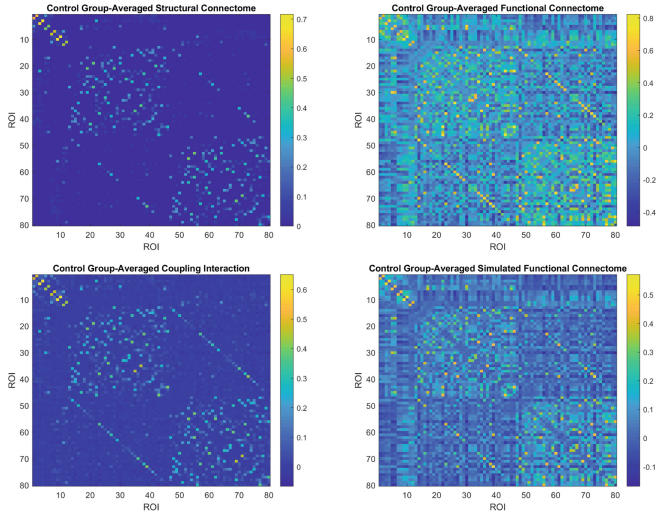

Fig. 2. Control group-averaged plots: Structural connectome in the *top left*, and coupling interaction network in the *bottom left* with Pearson correlation $r(|J|, SC) = 0.9493$, the observed functional connectome in the *top right* and the simulated functional connectome using our method (for optimal β, λ) in the *bottom right* with Pearson correlation $r = 0.9626$

One previous study using this data set computed standard graph theoretic metrics on the structural and functional networks. They found that carrier and control groups did not differ in measures of efficiency (global/local) or nodal centrality when analyzing the DTI or fMRI-derived networks separately [9]. Therefore, to investigate the significance of our estimated networks, we first compute the percent of positive and negative edges for each ROI in the signed rs-SC for each subject (control group), defined as p_c^+ and p_c^- for each ROI. For example, if an ROI has 45 positive edges and 34 negative edges, then $p_c^+ = \frac{45}{79}$ and $p_c^- = \frac{34}{79}$

ROIs with the 10 highest group-mean p_c^+ and p_c^- are shown in Fig. 3, the latter of which includes the anterior and rostral cingulate gyrus, caudate nucleus as well as the left thalamus. These are known regions with strong neural inhibitory influences on other ROIs. In particular, prefrontal cortical regions are strongly associated with cognitive control and response inhibition [2,8,10]. Sub-cortical structures including the caudate nuclei and thalamus also provide inhibitory control over motor functions through the cortico-basal ganglia-thalamo-cortical loop [13]. The correspondence between known inhibitory hubs and ROIs with higher incidence of negative interactions provides support for the insight our novel structure-function modeling may yield into the E-I balance.

We then define p_{e4}^+ similar to the control group and examine group differences between p_{e4}^+ and p_c^+ using a 2-sample T-test at the ROI-level, followed by FDR for multiple comparison correction ($q = 0.1$). This yielded 5 ROIs (shown in Fig. 3) with significant group differences. The left rostral anterior cingulate, left

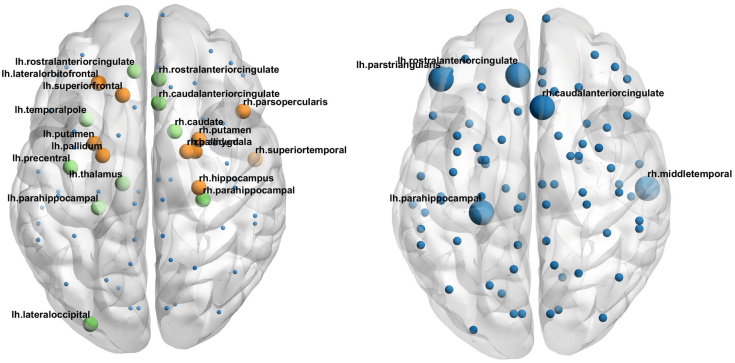

Fig. 3. Anatomical Nodes: *Left:* 10 largest group-mean p_c^+ (orange) and p_c^- (green). *Right:* ROIs with significantly higher p_{e4}^+ as compared to p_c^+ are the rostral anterior cingulate ($p = 2.598\text{e}{-3}$), parahippocampal ($p = 7.215\text{e}{-4}$), and pars triangularis ($p = 1.833\text{e}{-3}$) regions in the left hemisphere, as well as the caudal anterior cingulate ($p = 9.16\text{e}{-4}$) and middle temporal ($p = 5.359\text{e}{-4}$) regions in the right hemisphere. (Color figure online)

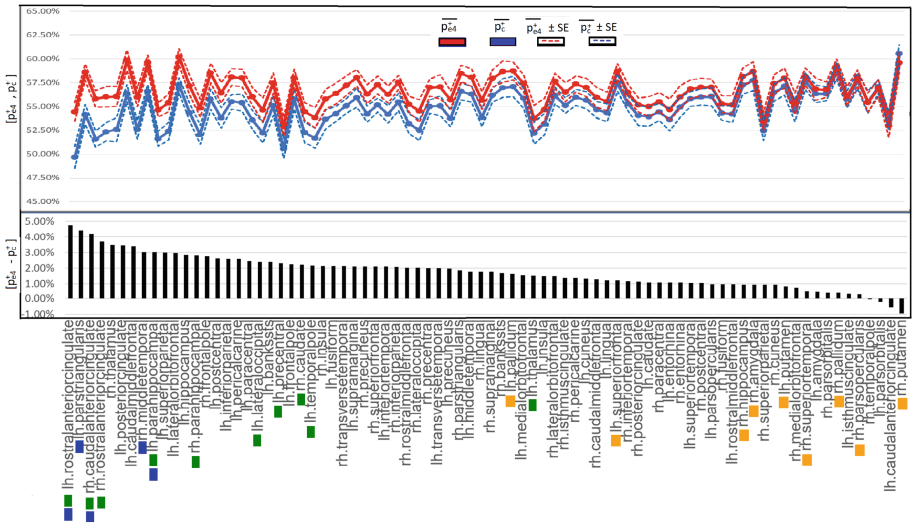

Fig. 4. Line Plots: Group-mean p_{e4}^+ and p_c^+ for each ROI, with ribbons for standard error (SE). Bar Plot: Difference between p_{e4}^+ and p_c^+. Green and Orange squares represent the 10 ROIs with the largest group-mean p_c^+ and p_c^-. Blue squares represent ROIs with significant group difference between p_{e4}^+ and p_c^+. Most ROIs in the APOE-e4 group have increased positive interactions as compared to the control group. Also, $\frac{3}{5}$ of the significant ROIs have higher p_c^- (rostral anterior cingulate, and the parahippocampal region in the left hemisphere and caudal anterior cingulate in the right hemisphere). (Color figure online)

parahippocampal, and right caudal anterior cingulate regions–are also among top p_c^-. Regions exhibiting the largest $[p_{e4}^+ - p_c^+]$ as shown in Fig. 4 tend to have fewer positive interactions in total, suggesting the presence of a shift from negative to positive interactions. Significant group differences were identified in regions of the anterior cingulate gyrus, middle temporal gyrus, inferior frontal gyrus and parahippocampal region. Moreover, white matter volume changes linked to APOE e4 [5] could also imply an increased risk for hyperexcitation, specifically in ROIs we identified after FDR correction (e.g. anterior cingulate).

5 Conclusion

We have presented here a method for estimating the positive and negative interactions between brain regions by creating a new connectome, the signed rs-SC, that embeds functional data onto a given structure. The resulting networks were validated on a sample of APOE-e4 carriers and non-carriers. When comparing the networks of the two groups, our approach identified a global shift in the E-I balance of the APOE e4 signed rs-SC as compared to the control group, thus providing the first connectomics-based support for the hyperexcitation hypothesis of AD. Future work would involve a deeper investigation into the E-I balance, including subjects with MCI and mild AD Dementia.

Acknowledgements. This study is funded in part by NIA AG056782 and NSF-IIS 1837956.

References

1. Ackley, D.H., Hinton, G.E., Sejnowski, T.J.: A learning algorithm for Boltzmann machines. Cogn. Sci. **9**(1), 147–169 (1985)
2. Badre, D., Wagner, A.D.: Selection, integration, and conflict monitoring; assessing the nature and generality of prefrontal cognitive control mechanisms. Neuron **41**, 473–487 (2004)
3. Besag, J.: Statistical analysis of non-lattice data. Statistician **24**(3), 179 (1975)
4. Binder, K., Heermann, D.W.: Monte Carlo Simulation in Statistical Physics: An Introduction. Springer, Heidelberg (2010). https://doi.org/10.1007/978-3-642-03163-2
5. Dowell, N.G., Evans, S.L., Tofts, P.S., King, S.L., Tabet, N., Rusted, J.M.: Structural and resting-state MRI detects regional brain differences in young and mid-age healthy APOE-e4 carriers compared with non-APOE-e4 carriers. NMR in Biomed. **29**(5), 614–624 (2016)
6. Ezaki, T., Watanabe, T., Ohzeki, M., Masuda, N.: Energy landscape analysis of neuroimaging data. Philos. Trans. R. Soc. A Math. Phys. Eng. Sci. **375**(2096), 20160287 (2017)
7. Fraiman, D., Balenzuela, P., Foss, J., Chialvo, D.R.: Ising-like dynamics in large-scale functional brain networks. Phys. Rev. E **79**(6), 061922 (2009)
8. Koechlin, E., Ody, C., Kouneiher, F.: The architecture of cognitive control in the human prefrontal cortex. Science **302**, 1181–1185 (2003)

9. Korthauer, L., Zhan, L., Ajilore, O., Leow, A., Driscoll, I.: Disrupted topology of the resting state structural connectome in middle-aged APOE ε4 carriers. Neuroimage **178**, 295–305 (2018)
10. MacDonald 3rd, A.W., Cohen, J.D., Stenger, V.A., Carter, C.S.: Dissociating the role of the dorsolateral prefrontal and anterior cingulate cortex in cognitive control. Science **288**, 1835–1838 (2000)
11. Marinazzo, D., Pellicoro, M., Wu, G., Angelini, L., Cortés, J.M., Stramaglia, S.: Information transfer and criticality in the ising model on the human connectome. PLoS ONE **9**(4), e93616 (2014)
12. Nguyen, H.C., Zecchina, R., Berg, J.: Inverse statistical prob-lems: from the inverse Ising problem to data science. Adv. Phys. **66**(3), 197–261 (2017)
13. Parent, A., Hazrati, L.: Functional anatomy of the basal ganglia. I. the cortico-basal ganglia-thalamo-cortical loop. Brain Res. Rev. **20**(1), 91–127 (1995)
14. Petrache, A.L.: Aberrant excitatory-inhibitory synaptic mechanisms in entorhinal cortex microcircuits during the pathogenesis of alzheimer's disease. Cereb. Cortex **29**(4), 1834–1850 (2019)
15. Ren, S., et al.: Amyloid β causes excitation/inhibition imbalance through dopamine receptor 1-dependent disruption of fast-spiking GABAergic input in anterior cingulate cortex. Sci. Rep. **8**(1), 302 (2018)
16. Schneidman, E., Berry, M.J., Segev, R., Bialek, W.: Weak pairwise correlations imply strongly correlated network states in a neural population. Nature **440**(7087), 1007–1012 (2006)
17. Watanabe, T., et al.: A pairwise maximum entropy model accurately describes resting-state human brain networks. Nat. Commun. **4**(1), 1370 (2013)
18. Yeh, F., et al.: Maximum entropy approaches to living neural networks. Entropy **12**(1), 89–106 (2010)